ACADEMIC PRESS

Available online at www.sciencedirect.com

SCIENCE DIRECT®

Journal of Structural Biology 139 (2002) 171–180

Journal of Structural Biology

www.academicpress.com

Three-dimensional structure of manganese superoxide dismutase from *Bacillus halodenitrificans*, a component of the so-called "green protein"

Jun Liao,[a] Ming-Yih Liu,[b] Tschining Chang,[c] Mei Li,[a] Jean Le Gall,[b] Lu-Lu Gui,[a] Ji-Ping Zhang,[a] Tao Jiang,[a] Dong-Cai Liang,[a] and Wen-Rui Chang[a,*]

[a] *National Laboratory of Biomacromolecules, Institute of Biophysics, Chinese Academy of Sciences, 15 Datun Road, Chaoyang District, Beijing 100101, China*

[b] *Department of Biochemistry and Molecular Biology, University of Georgia, Athens, GA 30602-7229, USA*

[c] *Institute of Biological Chemistry, Academia Sinica, Taipei 11529, Taiwan*

Received 6 May 2002, and in revised form 12 September 2002

Abstract

A so-called "green protein" has been purified from a moderate halophilic eubacterium, *Bacillus halodenitrificans* (ATCC 49067), under anaerobic conditions. The protein, which might play an important role in denitrification, dissociates mainly into two components after exposure to air: a manganese superoxide dismutase (GP-MnSOD) and a nucleoside diphosphate kinase. As a first step in elucidating the overall structure of the green protein and the role of each component, the 2.8-Å resolution crystal structure of GP-MnSOD was determined. Compared with other manganese dismutases, GP-MnSOD shows two significant characteristics. The first is that the entrance to its substrate channel has an additional basic residue—Lys38. The second is that its surface is decorated with an excess of acidic over basic residues. All these structural features may be related to GP-MnSOD's high catalytic activity and its endurance against the special cytoplasm of *B. halodenitrificans*. The structure of GP-MnSOD provides the basis for recognizing its possible role and assembly state in the green protein.

Keywords: Anaerobic; Catalytic activity; Denitrification; Electrostatic guidance; Halophilic

1. Introduction

Bacillus halodenitrificans (*Bh*)[1] (ATCC 49067), a moderate halophile, facultative anaerobe, and gram-positive denitrifier, reduces both nitrate and nitrite to nitrous oxide as the final denitrification product (Denariaz et al., 1989). A so-called "green protein" (which will be referred to as the green protein complex (GPC)) has been purified from this bacterium under anaerobic conditions. GPC, which contains protohemes and can reversibly bind nitric oxide (NO), probably plays an important role in the high tolerance of the organism toward nitrite (Denariaz et al., 1994). Following exposure to air, the complex loses its protohemes and dissociates into several polypeptide chains, two of which exhibit enzymatic activities: a manganese superoxide dismutase (GP-MnSOD) and a nucleoside diphosphate kinase (*Bh*NDK) (Le Gall et al., 2000). However, the details of the components' assembly and disassembly in GPC and the formation of their enzymatic forms are still unknown.

Superoxide dismutases (SOD) are critical for the protection of aerobic organisms against oxidative damage by disproportionating the superoxide radical to hydrogen peroxide and dioxygen (Beyer et al., 1991). Four types of SODs have been reported based on the metal species at the active site: (a) dinuclear Cu,Zn-SOD,

* Corresponding author. Fax: 86-10-64889867.
E-mail address: wrchang@sun5.ibp.ac.cn (W.-R. Chang).

[1] *Abbreviations used:* SOD, superoxide dismutase; rms, root mean square; *Bh*, *Bacillus halodenitrificans*; *Ec*, *Escherichia coli*; *Tt*, *Thermus thermophilus*; hm, human mitochondrial; GPC, green protein complex; GP-MnSOD, green protein manganese superoxide dismutase; *Bh*NDK, *Bh* nucleoside diphosphate kinase.

1047-8477/02/$ - see front matter © 2002 Elsevier Science (USA). All rights reserved.
PII: S1047-8477(02)00531-2

occurring primarily in eukaryotes; (b) FeSOD, found in prokaryotes; (c) MnSOD, existing in both prokaryotes and eukaryotes; and (d) NiSOD, recently discovered in *Streptomyces griseus* (Youn et al., 1996) and *S. coelicolor* (Kim et al., 1996). To date, some structures have been reported for FeSOD, MnSOD, and Cu,Zn-SOD. MnSODs and FeSODs are homologous to each other. They are generally dimers or tetramers, with each monomer being folded into an N-terminal helical domain and a C-terminal α/β domain (Stallings et al., 1984). Cu,Zn-SOD is generally a dimer with each subunit showing a Greek key β-barrel fold (Tainer et al., 1982).

As a dissociated component of GPC in the presence of air, GP-MnSOD has a number of unsolved problems, including its assembly in GPC and its role in the whole cell. In addition, the structural elements related to this homodimeric enzyme's relatively high catalytic activity (Denariaz et al., 1990) and its adaptation to the special cytoplasm of *Bh* are unknown. This paper presents the crystal structure of GP-MnSOD at 2.8 Å resolution, highlighting structural elements contributing to the enzyme's activity and stability. The structure of GP-MnSOD provides the basis for recognizing its possible role and assembly state in GPC.

2. Materials and methods

2.1. Proteins

Bh was grown as previously described (Denariaz et al., 1994). GP-MnSOD and GPC were purified under aerobic and anaerobic conditions, respectively (Denariaz et al., 1990, 1994). No SOD activity can be detected in fresh GPC. However, after exposure to air, SOD activity can be assayed in its dissociated polypeptides.

2.2. Crystallization and data collection

GP-MnSOD was crystallized at 9 °C by the hanging drop vapor diffusion method. The crystals were obtained by mixing 2 μl of the enzyme solution (6 mg/ml, 20 mM sodium cacodylate at pH 6.5) with an equal volume of the reservoir solution: 10% (w/v) polyethylene glycol 4000, 100 mM sodium cacodylate (pH 6.5), and 10 mM zinc acetate. Crystals appeared within 2 weeks and grew to $0.2 \times 0.2 \times 0.2$ mm in size. With a crystal-to-detector distance of 120 mm, a 250° data set (1° oscillation frames) was collected at room temperature on a Mar Research Image Plate System using monochromated Cu Kα radiation. The intensities between 20.0 and 2.8 Å were integrated with the program DENZO and scaled with the program SCALEPACK (Otwinowski and Minor, 1996). 7286 unique reflections occupying each reflection shell in full were obtained, among which 5994 reflections had densities higher than $2\sigma_I$. The systematic absence of reflections showed that the space group belonged to $P4_32_12$ or $P4_12_12$, with cell dimensions $a = b = 93.1$ Å and $c = 63.5$ Å. Calculations based on the Matthews method (Matthews, 1968) gave one SOD monomer in an asymmetric unit with an expected solvent content of 59%. Details of the data processing statistics are given in Table 1.

2.3. Structure determination

The initial phases were solved by the molecular replacement method with the program AMoRe (Navaza, 1994) using a subunit of *Thermus thermophilus* MnSOD (*Tt*MnSOD; PDB ID: 3mds, 1.8 Å, 55% sequence identity with GP-MnSOD) (Ludwig et al., 1991) as the probe. Rotation and translation function searches were calculated in the resolution range between 8.0 and 3.5 Å. The rotation search gave a single cross-rotation solution that correlated well with the calculated crystal density. Translation searches using the rotation angle solution resulted in an unambiguous position of the monomer in space group $P4_32_12$ with a correlation coefficient of 55.6%, an R value of 41.6%, and reasonable packing.

The GP-MnSOD model was subsequently built using the graphic program O (Jones et al., 1991) and refined against the data ($F > 2\sigma_F$) between 10 and 2.8 Å using the program CNS1.0 (Brünger et al., 1998). Ten percent of the reflections were selected randomly to check the course of refinement by calculating the R_{free} value (Brünger, 1992). The temperature factors were initially set to 20.0 Å^2. To avoid imposing a certain metal geometry, the geometry of the metal atom was restrained only by nonbond interactions. At first, five cycles of model rebuilding were carried out. Most of the atoms, including manganese and zinc atoms, were fitted to simulated annealing omit Fourier maps (Hodel et al., 1992). After model rebuilding, the R value dropped to 33.7%. A subsequent round of simulated annealing refinement using the torsion angle dynamic slow-cooling protocol (Rice and Brünger, 1994) reduced the R value to 28.7%. Subsequent cycles of positional refinement, unrestrained group B factors, and restrained individual isotropic B factors refinement further improved the model quality and reduced the R factors. At this stage, water molecules were identified as peaks in $(F_o - F_c)$ and $(2F_o - F_c)$ density maps using a cutoff of 3σ and 1σ, respectively. Water molecules were included in the model only when they were within hydrogen bond distance to appropriate atoms. The final model of the GP-MnSOD monomer included 201 residues (Lys2–Ala202), a manganese atom, a zinc atom, and 63 water molecules with a crystallographic R factor of 22.0% and a free R factor of 28.9% (Table 1). The N-terminal and C-terminal residues were not visible in the $2F_o - F_c$ electron density maps. No side-chain electron densities could be seen for Lys2, Lys108, Lys114, or Asn138 in the final structure. The rms deviations from ideal values of the bond lengths

Table 1
Crystal diffraction data and structural statistics of GP-MnSOD

Crystal data		
Wavelength	1.54 Å	
Resolution range (Å)	20–2.8 M	
Space group	$P4_32_12$	
Unique reflections[a]	5994	
Completeness (%) (outermost shell)[a]	82.3 (54.3)	
I/σ_I (outermost shell)	24.2 (3.6)	
Average redundancy	19.3	
R_{merge} (%)[a]	9.5	
Unit-cell parameters	$a = b = 93.1$ Å, $c = 63.5$ Å	
Refinement results	R[b]	R_{free}[b]
Initial model (%) (10–2.8 Å)	45.0%	
After refinement (10–2.8 Å)	22.0%	28.9%
Overall temperature factor (Å^2) (main chain/side chain/all protein atoms)	23.9/25.3/24.6	
R_{msd} bond length (Å)	0.009	
R_{msd} bond angles (°)	1.446	
Total number of amino acid residues/unit	201	
Total number of atoms (non-hydrogen)	1582	

$R_{merge} = \sum_h \sum_i [|I_i(h) - \langle I(h)\rangle|/\sum_h \sum_i I_i(h)]$, where I_i is the ith measurement and $\langle I(h)\rangle$ is the weighted mean of all measurements of $I(h)$. The outermost shell is 2.86–2.80 Å.

[a] Reflections of $2\sigma_I$ cutoff were applied in generating the statistics.

[b] $R = \sum_h |F_o - F_c|/\sum_h F_o$, where F_o and F_c are the observed and calculated structure factor amplitudes of reflection h.

and bond angles were 0.009 Å and 1.446°, respectively. As defined in the program PROCHECK (Laskowski et al., 1993), no main-chain dihedral angle was observed in disallowed regions of the Ramachandran plot (Ramachandran and Sasisekharan, 1968) and most (98.3%) of the dihedral angles were found in the most favored and additional allowed regions. Structure factors and coordinates have been deposited in the RCSB Protein Data Bank under Accession Code 1JR9.

2.4. Analysis of data

Secondary structures were assigned according to the Kabsch and Sander algorithm (Kabsch and Sander, 1983). The solvent-accessible surface areas were calculated with the surface option in the program CNS1.0 (Brünger et al., 1998) according to the algorithm of Lee and Richard (Lee and Richard, 1971). During the calculation, a probe radius of 1.4 Å was applied and all solvent molecules were excluded. Hydrogen bonds were analyzed with the program WHATIF (Vriend, 1990). The structural-based sequence alignment was done with the least-squares approach implemented in program O (Jones et al., 1991).

3. Results and discussion

3.1. Monomer and the active site structures

The molecular weight of the GP-MnSOD monomer determined by electron spray ionization mass spectroscopy was 22.9 kDa. The amino acid sequence from Ala1 to Ala195 was deduced from the cDNA analysis, while a proposed His18, inconsistent with the electron density, was corrected to a threonine by Edman degradation. The C-terminal sequence after Ala195 was modeled according to the electron density and homologous sequences.

The GP-MnSOD monomer comprises the general fold of Mn/Fe-dependent dismutases, with an N-terminal helical domain and a C-terminal α/β domain (Figs. 1 and 2a). The N-terminal domain (Lys2–Asn92) contains two long α helices (α1 and α3) connected by the loop L2 (Gly41–Pro65). Residues from Lys2 to Asp13 in loop L1 (Lys2–Asp20) have an extended structure packed against helices α1 and α3. The first long helix α1 (Lys21–Asn40) is distorted at Lys30 with ϕ and ψ angles of −115.7° and −86.5°. This distortion, which has been described in *Tt*MnSOD (Stallings et al., 1985), moves the conserved Tyr35 near to the active site. As shown by site-directed mutagenesis, Tyr35 is crucial for maintaining the enzyme activity and the integrity of the active site (Hunter et al., 1997). Loop L2 connecting helices α1 and α3 contains a short helix, α2, and bends toward the C-terminal domain with a conformation similar to that of *Tt*MnSOD (Ludwig et al., 1991).

The C-terminal domain (Gly93–Ala202) is of the α + β type and consists of a triple-stranded antiparallel β sheet with helices α4, α5, α6, and α7 on one side and a loop joining strands β2 and β3 on the other. The β2 strand (five residues) of GP-MnSOD is relatively shorter than those (seven or eight residues) of other manganese dismutases, including *Tt*MnSOD,

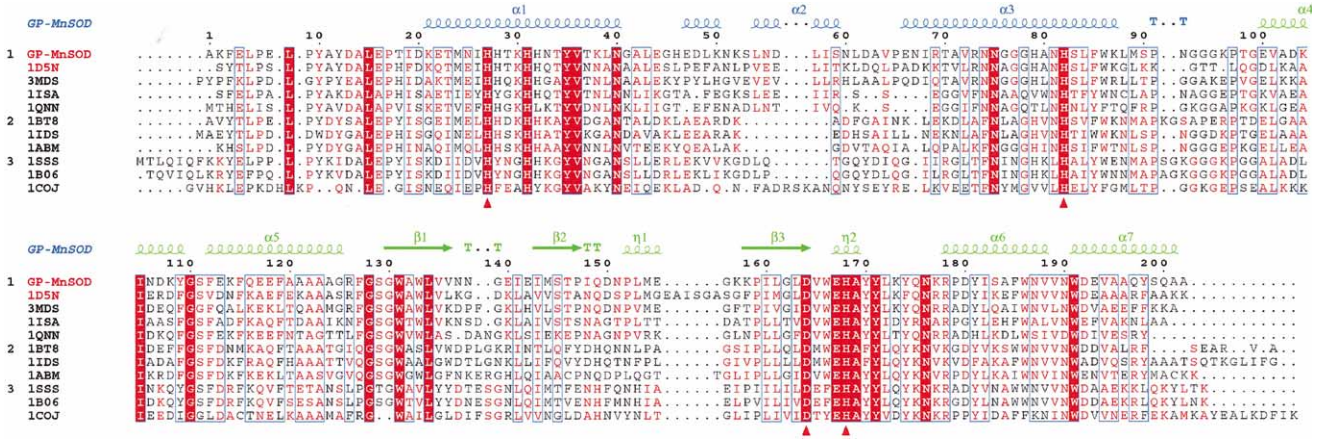

Fig. 1. Structure-based sequence alignment of known Mn/FeSOD structures. The first line shows the secondary structural assignments of the N-terminal domain (blue) and C-terminal domain (green) of GP-MnSOD: α, α helix; β, β strand; TT, turn; $\eta, 3_{10}$ helices. One α helix in the loop 2 region is not marked due to its short length. The SODs are divided into three groups (marked on the left side) according to their sources and the conformation of the loop 2 regions. Group 2 (eubacteria) and group 3 (archaebacteria) have similar conformations in the loop 2 regions. GP-MnSOD and *Ec*MnSOD are colored red for their highest identity (56%). The ligands of the active-site metal are marked with red triangles. The residues are colored as red box and white character, strict identity; red character, similarity within a group; blue frame, similarity across groups. The figure was produced with the program ESPript 1.9 (Gouet et al., 1999). PDB accession codes: 1d5n, *Ec* MnSOD; 3mds, *Tt*MnSOD; 1isa, *Ec* FeSOD; 1qnn, *P. gingivalis* cambialistic SOD; 1bt8, *P. shermanii* cambialistic SOD; 1ids, *M. tuberculosis* FeSOD; 1abm, hmMnSOD; 1sss, *S. solfataricus*FeSOD; 1b06, *S. acidocaldarius* FeSOD; 1coj, *A. pyrophilus* FeSOD.

Escherichia coli MnSOD (*Ec*MnSOD; PDB ID: 1d5n), and human mitochondrial MnSOD (hmMnSOD; PDB ID: 1abm) (Borgstahl et al., 1992, 2000; Ludwig et al., 1991).

The active-site manganese joins the two domains together. Two amino acid residues from each domain, His27 in α1 and His82 in α3 from the N-terminal domain and Asp164 in β3 and His168 in loop L7 from the C-terminal domain, ligate the manganese atom (Table 2). The geometry of the binding can be described as a distorted tetrahedral arrangement with His27 at the apex, similar to that of *Bacillus stearothermophilus* MnSOD (Parker and Blake, 1988). As in other dismutases, the manganese is buried in a relatively hydrophobic environment: in the proximity of the manganese (7 Å cutoff), residues His31, Tyr35, Phe85, Trp86, Trp131, Gln149, and Trp166, as well as Glu167 from the neighboring monomer in a functional dimer, can be found. The ND1 of manganese ligand His168 makes a hydrogen bond (bond length ~2.8 Å) to the OE2 of Glu167 from the neighboring monomer in a functional dimer. Although this structural feature is highly conservative in dismutases, its significance is unknown. One suggestion is that these residues form bridges for communication between the two active sites (Edwards et al., 1998).

3.2. Quaternary structure

There is only one monomer in an asymmetric unit of GP-MnSOD. Two monomers related by the crystallographic twofold axis in the *xy* direction form a functional homodimer. In contrast, subunits in a functional dimer of any other manganese dismutase are related by a noncrystallographic dyad axis (Borgstahl et al., 1992, 2000; Edwards et al., 1998; Ludwig et al., 1991; Parker and Blake, 1988). Despite the above-stated difference, the assembly of the functional dimers is similar (Fig. 2b): the rms deviations between the GP-MnSOD dimer and those of *Ec*MnSOD, *Tt*MnSOD, and hmMnSOD are 0.904, 0.945, and 0.805 Å for 385, 396, and 362 equivalent α-carbon atoms, respectively.

The active-site manganeses of the two GP-MnSOD monomers are located near the dimer interface with a distance of 18.0 Å. The dimer interactions involve residues from helices α1 (22, 26, 30, 31, 35), α3 (74), the loop (127–129) joining α5 and β1, the loop (148) joining β2 and β3, and the loop (166–168, 171, 172, 175, 176) joining β3 and α6. Among all 17 of these residues (from each monomer) containing 53% polar residues, 29% hydrophobic residues, and 18% charged residues, 15 are conserved, with 11 identical in all manganese dismutases (Fig. 1). Such conservation may be crucial in maintaining the specialty and stability of the dimer interface, which has a total of 1713 Å^2 of buried surface area in GP-MnSOD. Most of the interactions at the dimer interface are hydrophobic. Residues Asn74 from one monomer and Phe127 from the neighboring monomer form an amino/aromatic stacking-type interaction across the dimer interface with the ND2… ring carbon distance of approximately 3.7 Å. All contacts at the dimer interface are duplicated by the crystallographic twofold axis.

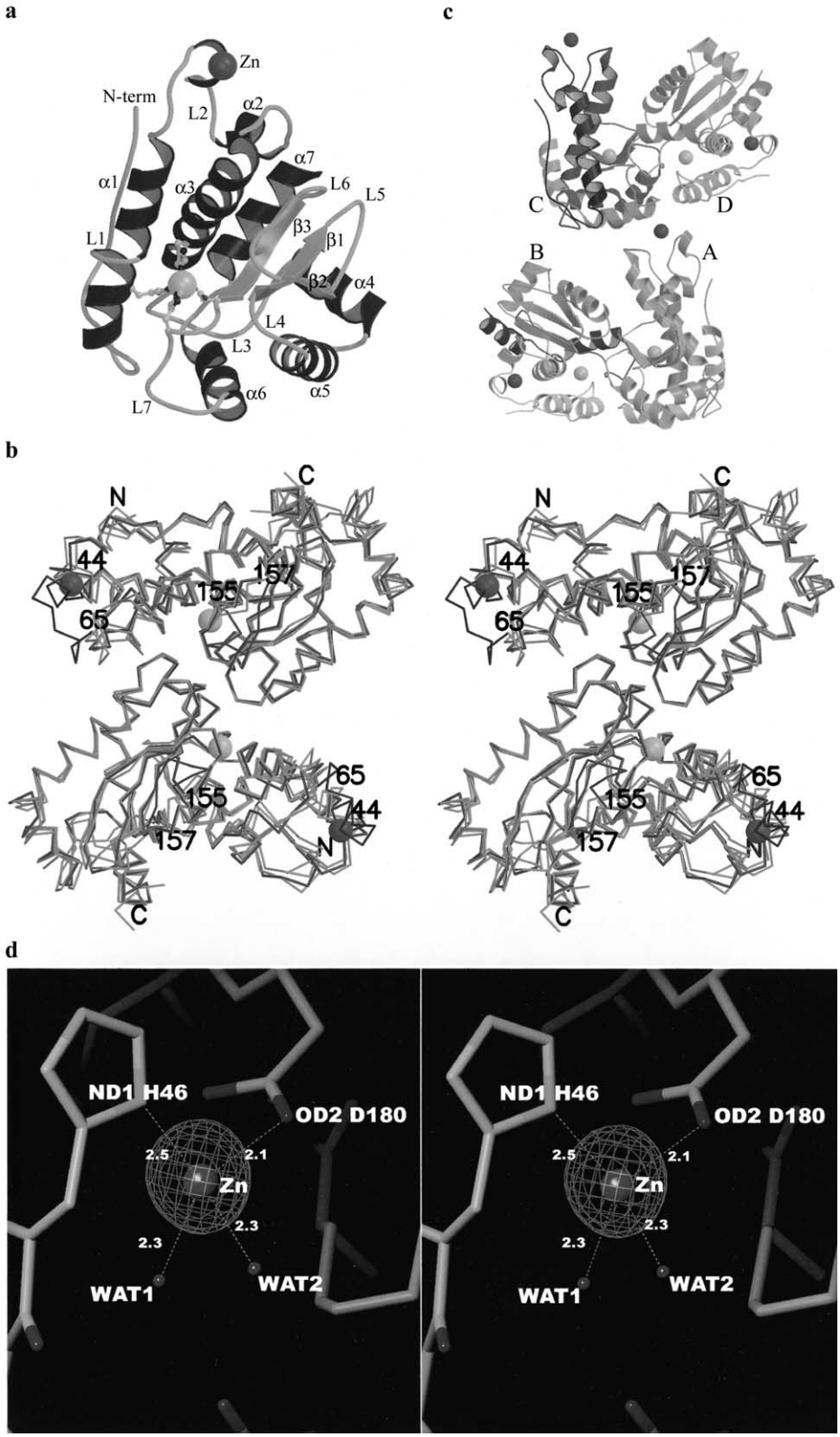

Fig. 2. GP-MnSOD monomer fold, dimer fold, and zinc site arrangement. (a) Overall monomer structure. There is one monomer and an additional zinc atom in an asymmetric unit of GP-MnSOD. (b) Stereoview of superimposed α-carbon traces of functional dimers of GP-MnSOD (thick and dark), hmMnSOD, *Tt*MnSOD, and *Ec*MnSOD. Also shown are two large disparities between hmMnSOD (residues 44–65) and GP-MnSOD and between *Ec*MnSOD (additional loop between positions 155 and 157) and GP-MnSOD. (c) The zinc atom between monomers of neighboring dimers. His46 from monomer A and Asp180 from monomer C ligate zinc. (d) Stereoview of the $F_o - F_c$ electron density map at the zinc site. The map was calculated with the zinc ion and neighboring atoms ($\leqslant 3.5$ Å) omitted and was contoured at a 12σ level. (a)–(c) Drawn using the programs MOLSCRIPT (Kraulis, 1991) and RASTER3D (Merritt and Murphy, 1994). (d) Prepared with the program TURBO–FRODO (Jones, 1978).

Table 2
Geometry of the metal-binding sites in GP-MnSOD

	Mn		Zn
Distance (Å)			
His27 N^{E2}	2.0	H_2O1	2.3
His82 N^{E2}	2.1	H_2O2	2.3
Asp164 O^{D2}	2.1	His46 N^{D1}	2.5
His168 N^{E2}	1.9	Aspl80 O^{D2} [a]	2.1
Angles (°)			
N^{E2} (27)–M–N^{E2} (82)	85.2	O (1)–M–O (2)	79.3
N^{E2} (27)–M–O^{D2} (164)	91.8	O (1)–M–N^{D1} (46)	129.9
N^{E2} (27)–M–N^{E2} (168)	92.6	O (1)–M–O^{D2} (180)[a]	130.9
N^{E2} (82)–M–O^{D2} (164)	76.7	O (2)–M–N^{D1} (46)	108.8
N^{E2} (82)–M–N^{E2} (168)	146.4	O (2)–M–O^{D2} (180)[a]	100.9
O^{D2} (164)–M–N^{E2} (168)	136.9	N^{D1} (46)–M–O^{D2} (180)[a]	97.0

[a] Asp180 is from another monomer generated by the symmetry operator of $1/2 - x, 1/2 + y, 3/4 - z$.

3.3. The zinc atom between monomers of neighboring dimers

The difference Fourier maps showed a high positive peak near ND1 of His46, with a height about the same as that of the manganese atom during the model rebuilding stage. Due to the presence of zinc acetate in the crystallization recipe and the zinc characteristic absorption in atomic absorption spectroscopy analysis, the peak was modeled as a zinc atom. After the addition of the zinc atom, subsequent refinements converged smoothly. The coordination of the zinc atom is tetrahedral and has four ligands (Fig. 2c and d; Table 2). The ligands are two water molecules, ND1 of His46 from one monomer and OD1 of Asp180 from another monomer of a neighboring dimer which is symmetrically related to the former monomer by the axis along the *y* direction. This is the first report in Fe/Mn-dependent dismutases that a zinc atom lies at the interface between two monomers. Its significance for GP-MnSOD remains unknown, except that the zinc atom can stabilize the crystal packing.

3.4. Substrate channel

As in *Tt*MnSOD (Ludwig et al., 1991), two symmetric substrate channels, via which the superoxide radicals and substrate molecules reach the active sites, lie at the dimer interface in GP-MnSOD. Each channel is approximately 7 Å in depth and approximately 11 Å in diameter and includes three layers of residues from the surface to the active site: the channel entrance is composed of Lys30, Thr34, Thr37, and Lys38, as well as Arg126, Phe127, and Lys177 from the neighboring monomer; as the substrate molecule approaches the active site, it meets with residues Ser129 and Ser129 and Arg178 from the neighboring monomer; finally, the substrate will encounter His31, Tyr35, Trp131, Gln149, and Trp166, as well as Glu167 from the neighboring monomer. The dismutation of superoxide radicals by SOD is a reaction that is rate limited by diffusion and enhanced by electrostatic guidance: the arrangement of electrostatic charges in SOD promotes productive enzyme–substrate interaction through substrate guidance and charge complementarity (Getzoff et al., 1992; Ludwig et al., 1991; Sines et al., 1990). So, the arrangement of basic residues at or around the substrate channel of GP-MnSOD may significantly influence the catalytic reaction rate. The conservation of the basic residues lining the substrate channel decreases with the increment of distances between their basic groups and the manganese atom (Table 3, Fig. 1). The conservation of basic residues as well as their distances to the metal center probably reflect their different roles in electrostatic guidance: the closest and most conservative Arg178 may play a leading role; farther and less conservative Lys30 may have a weaker effect; the farthest and most variable Arg126 and Lys177 may have the weakest influence.

3.5. Structural characteristics related to the high catalytic activity

The catalytic activity of GP-MnSOD, expressed as the amount of enzyme inhibiting by 50% the reduction of cytochrome *c*, is 5150 units $\cdot$ mg^{-1}, which is higher than those of reported manganese dismutases (Denariaz et al., 1990; Gorecki et al., 1991; Ludwig et al., 1991). The high activity of GP-MnSOD is probably related to its two distinctive characteristics: an additional basic residue—Lys38 at its channel entrance and an excess of acidic over basic residues on the protein surface (Fig. 3a–d, Tables 3 and 4).

Lys38 may increase the enzyme–substrate association rate by enhancing the electrostatic gradient (Borders et al., 1989; Getzoff et al., 1992; Sines et al., 1990). Lys38 may also facilitate the enzyme–substrate recognition process in other aspects: First, in previously reported MnSOD structures (Borgstahl et al., 1992, 2000; Ludwig

Table 3
Basic residues along the substrate channel in manganese superoxide dismutases from GPC, *Ec* (Borgstahl et al., 2000), *Tt* (Ludwig et al., 1991), and hm (Borgstahl et al., 1992)

	Lys30	Lys38	Arg126[a]	Lys177[a]	Arg178[a]
GPC	13.8	15.7	17.7	17.2	12.7
Ec	14.7	Asn38[b]	17.5	16.2[c]	12.9
Tt	15.0	Asn38[b]	17.7	16.9[c]	13.1
hm	14.7	Asn38[b]	Val126[b]	16.7[d]	12.7

The values are average distances (Å) between the basic groups and the manganese atom. All basic residues within 18 Å were included. They were numbered according to the sequence of GP-MnSOD in Fig. 1.

[a] Residues of the neighboring monomer in a functional dimer.

[b] For uncharged residues, values are not presented.

[c] The value for Arg177.

[d] The value for Arg175.

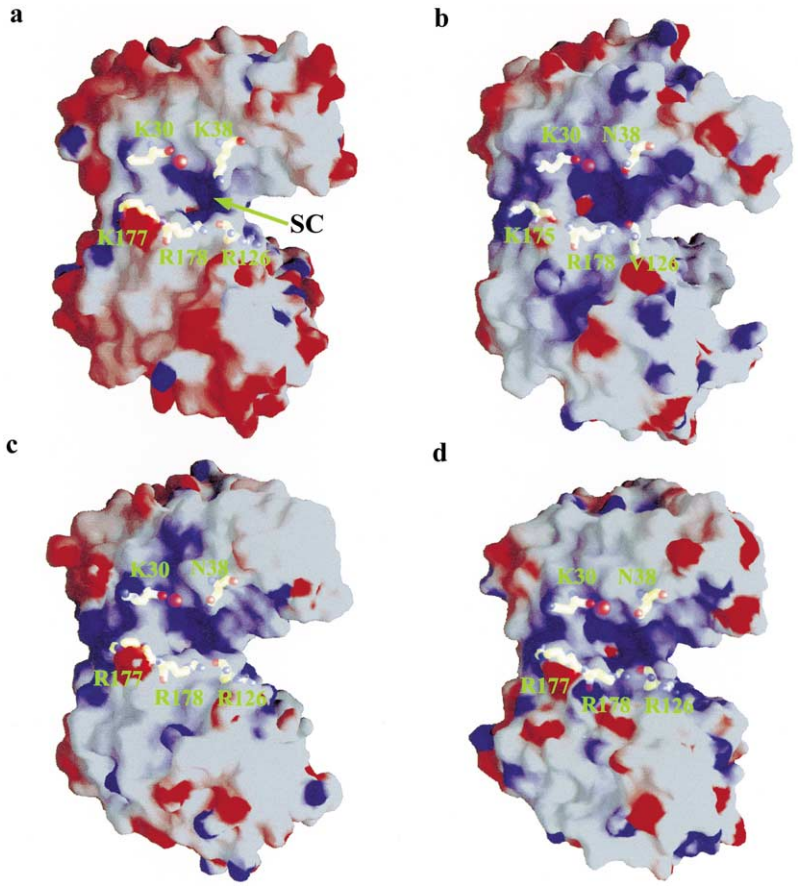

Fig. 3. Comparative views of GP-MnSOD (a) with hmMnSOD (b), *Tt*MnSOD (c), and *Ec*MnSOD (d) on their functional dimers' surfaces and substrate channels. All molecules are viewed along one of the substrate channels in the same direction. SC, the substrate channel. Violet sphere, the manganese atom. The surfaces are colored according to the electrostatic potential with the program GRASP (Nicholls et al., 1991) (salt concentration, 0 M; red, negative; blue, positive; scale (-10 to $+10\,kTe^{-1}$)).

et al., 1991), basic residues at the channel entrance, including Lys30, Lys/Arg177, and Arg126, are arranged in an incomplete circle, in contrast to a full circle in GP-MnSOD, due to the additional Lys38 (Figs. 3a–d). Because of its possible long-range guidance effect (Gabbianelli et al., 1997; Sines et al., 1990), Lys38 may direct additional superoxide radicals to the channel entrance of GP-MnSOD. Second, the distance between the basic groups of Lys38 and Arg178 is about 11.0 Å, longer than that between Arg178 and Arg126 (~9.4 Å) but shorter than that between Arg178 and Lys30 (~16.7 Å) or between Arg178 and Lys177 (~12.9 Å). Since Arg178 plays a crucial role in electrostatic guidance (Gabbianelli et al., 1997), the relative short distance between Lys38 and Arg178 may facilitate superoxide anions in the proximity of Lys38 toward the active site.

Table 4
Net charge densities of manganese superoxide dismutases from GPC, *Ec*, *Tt*, and hm

	GPC	*Ec*	*Tt*	hm
Oligomerization state	Dimer	Dimer	Tetramer	Tetramer
Net charges on the surface	−14	−2	−8	0
Accessible surface area (Å^2)	17 583	17 169	32 038	31 187
Net charge density $\times 10^3$ (Å^{-2})	−0.80	−0.12	−0.25	0.00

Residue 38 varies from long-tail Lys and Asn to low-polar Gly among eubacterial Mn/FeSODs and hmMnSOD (Fig. 1). However, with the exception of the above variances, structural superposition shows little difference in the active site and the substrate channel in the dismutases. This means that local changes at residue 38 have little effect on the structural integrity of the active site and substrate channel, and Lys38 may purely play an electrostatic attractive role in GP-MnSOD, somewhat similar to that of human Cu,Zn-SOD (Getzoff et al., 1992). In that case, the catalytic activity was effectively increased with the increment of positive charges at the active site when its structural integrity was maintained.

The second structural element possibly contributing to the high catalytic activity of GP-MnSOD originates from an excess of acidic over basic residues on its surface, in contrast to the approximately equal number of acidic and basic residues in other MnSODs. GP-MnSOD, with 50 carboxylates covering the entire surface except the vicinity of the substrate channel, has the highest negative charge density among manganese dismutase structures (Table 4). Whereas other dismutases display both positive and negative isopotential surfaces, the GP-MnSOD is covered by an unusually large negative isopotential surface (Figs. 3a–d). This may enhance the reaction rate by reducing futile collisions of superoxide radicals with the surface (Benovic et al., 1983; Borders et al., 1989; Sines et al., 1990).

The rate-accelerating factors mentioned above are neither exhaustive nor mutually exclusive. It is entirely possible that all of the above factors, or some combination thereof, cause GP-MnSOD to exhibit high catalytic activity. Fully discerning the reasons behind GP-MnSOD's high activity should offer greater insight into the catalytic mechanism of dismutases.

3.6. Weak salt tolerance

Although halophilic archaebacteria and eubacteria have generally evolved two different osmotic strategies for adapting to extracellular hypersaline environments (Eisenberg et al., 1992; Ventosa et al., 1998), the salt concentration change in halophilic eubacteria has been observed to obey the general rule that the intracellular K^+ concentration is usually higher than that in the medium and the apparent intracellular Na^+ and K^+ concentrations increase nonlinearly with increasing external NaCl concentration. In addition, it has been observed that the apparent intracellular salt concentrations can reach very high levels in some halophilic eubacteria (Kamekura and Onishi, 1982; Weisser and Trüper, 1985). Since *Bh* can survive and multiply in media ranging in salinity from 0.35 to 4.25 M NaCl, and its salt requirement can be provided by 1 M KNO_3 or KCl instead of NaCl (Denariaz et al., 1989), the cytoplasm of *Bh* has a high concentration of salts, including at least 1 M KCl.

For halophilic proteins, an excess of acidic over basic residues distributed on their surface has been generally interpreted as a structural feature related to their salt tolerance (Elcock and McCammon, 1998; Madern et al., 1995, 2000). Compared with its homologues, GP-MnSOD shows a significant excess of acidic over basic residues on its surface (Table 4). So, GP-MnSOD may possess a certain degree of salt tolerance. However, the density of acidic residues on the surface of GP-MnSOD is lower than that in a typical halophilic protein. The difference in acidic residue content between GP-MnSOD and its nonhalophilic counterparts is also not statistically significant according to the criteria for halophilic proteins (Madern et al., 2000; Böhm and Jaenicke, 1994). Therefore, the salt-tolerance of GP-MnSOD is relatively weak.

3.7. Relationship with GPC

The function of GPC is not well understood. Since GPC can reversibly bind NO under anaerobic conditions through its mesoheme moieties, it has been proposed that GPC may function as a NO chelator to prevent the buildup of toxic free NO in denitrifying cells of *Bh* (Denariaz et al., 1994). The significance of the dissociation of GPC under aerobic conditions remains a puzzle. Since this dissociation results in the release of active *Bh*NDK and GP-SOD, it can represent an important protective mechanism against prompt twofold toxicity: the released GP-MnSOD can protect *Bh*NDK and other components against the damage of both superoxide radicals and peroxynitrites (Le Gall et al., 2000). Since the catalytic activity of SODs decreases with the impairment of electrostatic guidance when ionic strength increases (Benovic et al., 1983; Borders et al., 1989; Getzoff et al., 1992; Sines et al., 1990), the

additional Lys38 at the entrance to the substrate channel and the excess of acidic over basic residues on the surface may be crucial for GP-MnSOD to maintain enough activity in a saline cytoplasm of *Bh*.

The fact that GP-MnSOD and *Bh*NDK preexist as monomeric inactive forms in GPC under anaerobic conditions while they exhibit their activities after the exposure of GPC to air (Le Gall et al., 2000) probably represents a new regulation mechanism, which possibly also exists in aerobically exposed *Streptococcus faecalis*, in which a surge of SOD activities appears before any growth of the bacterium is detected (Gregory and Fridovich, 1973). The significance of the above mechanism is not well understood, though the de novo enzymatic synthesis is not required for GP-MnSOD and *Bh*NDK when *Bh* is exposed to air.

Since its molecular weight is far larger than that of any other dissociated polypeptide (M.-Y. Liu et al., unpublished data), GP-MnSOD may play a leading role in the assembly of GPC. There are no obvious differences between GP-MnSOD and other manganese dismutases, either in their monomer fold or in their dimer interaction, so it is hard to know how a monomer of GP-MnSOD participates in the assembly of GPC. GP-MnSOD monomer has two kinds of surfaces: the surface involved in dimerization and the surface away from the dimer interface. Since the former surface comprises a large amount of conservative uncharged residues and is near to the active site, it probably takes part in the assembly of the active site in GPC. Also, in this way, it may facilitate the manganese atom to exploit its function. The surface away from the dimer interface is covered with a large amount of negative charges. Therefore, it may be partially exposed so as to protect other parts in GPC against the detrimental influence of the saline cytoplasm.

Acknowledgments

The project was supported by the Key Project Foundation of the Chinese Academy of Sciences (Project KJ951-A1-601), the National Key Research Development Project of China (Project G1999075601), and National Institute of Health Grant GM 56000 (L.G. and M.Y.L.).

References

Benovic, J., Tillman, T., Cudd, A., Fridovich, I., 1983. Electrostatic facilitation of the reaction catalyzed by the manganese containing and the iron-containing superoxide dismutases. Arch. Biochem. Biophys. 221, 329–332.

Beyer, W., Imlay, J., Fridovich, I., 1991. Superoxide dismutases. Prog. Nucleic Acid Res. Mol. Biol. 40, 221–253.

Böhm, G., Jaenicke, R., 1994. Relevance of sequence statistics for the properties of extremophilic proteins. Int. J. Pept. Protein Res. 43, 97–106.

Borders, C.L., Horton, P.J., Beyer, W., 1989. Chemical modification of iron- and manganese-containing superoxide dismutases from *Escherichia coli*. Arch. Biochem. Biophys. 268, 74–80.

Borgstahl, G.E.O., Parge, H.E., Hickey, M.J., Beyer, W.F., Hallewell, R.A., Tainer, J.A., 1992. The structure of human mitochondrial manganese superoxide dismutase reveals a novel tetrameric interface of two 4-helix bundles. Cell 71, 107–118.

Borgstahl, G.E.O., Pokross, M., Chehab, R., Sekher, A., Snell, E.H., 2000. Cryo-trapping the six-coordinate, distorted-octahedral active site of manganese superoxide dismutase. J. Mol. Biol. 296, 951–959.

Brünger, A.T., 1992. Free *R* value: a novel statistical quantity for assessing the accuracy of crystal structures. Nature 355, 472–475.

Brünger, A.T., Adams, P.D., Clore, G.M., DeLano, W.L., Gros, P., Grosse-Kunstleve, R.W., Jiang, J.-S., Kuszewski, J., Nilges, M., Pannu, N.S., Read, R.J., Rice, L.M., Simonson, T., Warren, G.L., 1998. Crystallography and NMR system: a new software suite for macromolecular structure determination. Acta Crystallogr. D 54, 905–921.

Denariaz, G., Ketchum, P.A., Payne, W.J., Liu, M.-Y., Le Gall, J., Moura, I., Moura, J.J., 1994. An unusual hemoprotein capable of reversible binding of nitric oxide from the gram-positive *Bacillus halodenitrificans*. Arch. Microbiol. 162, 316–322.

Denariaz, G., Payne, W.J., Le Gall, J., 1989. A Halophilic Denitrifier, *Bacillus halodenitrificans* sp. nov. Int. J. Syst. Bacteriol. 39, 145–151.

Denariaz, G., Payne, W.J., Le Gall, J., 1990. Characterization of the superoxide dismutase of the denitrifying bacterium, *Bacillus halodenitrificans*. Biol. Met. 3, 14–18.

Edwards, R.A., Baker, H.M., Whittaker, M.M., Whittaker, J.W., Jameson, G.B., Baker, E.N., 1998. Crystal structure of *Escherichia coli* manganese superoxide dismutase at 2.1 Å resolution. J. Biol. Inorg. Chem. 3, 161–171.

Eisenberg, H., Mevarech, M., Zaccai, G., 1992. Biochemical, structural, and molecular genetic aspects of halophilism. Adv. Protein Chem. 43, 1–62.

Elcock, A.H., McCammon, J.A., 1998. Electrostatic contributions to the stability of halophilic proteins. J. Mol. Biol. 280, 731–748.

Gabbianelli, R., Battistoni, A., Polticelli, F., Meier, B., Schmidt, M., Rotilio, G., Desideri, A., 1997. Effect of Lys175 mutation on structure function properties of *Propionibacterium shermanii* superoxide dismutase. Protein Eng. 10 (9), 1067–1070.

Getzoff, E.D., Cabelli, D.E., Fisher, C.L., Parge, H.E., Viezzoli, M.S., Banci, L., Hallewell, R.A., 1992. Faster superoxide dismutase mutants designed by enhancing electrostatic guidance. Nature 358, 347–351.

Gorecki, M., Beck, Y., Hartman, J.R., Fischer, M., Weiss, L., Tochner, Z., Slavin, S., Nimrod, A., 1991. Recombinant human superoxide dismutases: production and potential therapeutical uses. Free Radic. Res. Commun. 12–13, 401–410.

Gouet, P., Courcelle, E., Stuart, D.I., Metoz, F., 1999. ESPript: multiple sequence alignments in PostScript. Bioinformatics 15, 305–308.

Gregory, E.M., Fridovich, I., 1973. Induction of superoxide dismutase by molecular oxygen. J. Bacteriol. 114, 543–548.

Hodel, A., Kim, S.-H., Brünger, A.T., 1992. Model bias in macromolecular crystal structures. Acta Crystallogr. A 48, 851–859.

Hunter, T., Ikebukuro, K., Bannister, W.H., Bannister, J.V., Hunter, G., 1997. The conserved residues tyrosine 34 is essential for maximal activity of iron-superoxide dismutase from *Escherichia coli*. Biochemistry 36, 4925–4933.

Jones, T.A., 1978. A graphics model building and refinement system for macromolecules. J. Appl. Crystallogr. 11, 268–272.

Jones, T.A., Zou, J.-Y., Cowan, S.W., Kjeldgaard, M., 1991. Improved methods for building protein models in electron density

maps and the location of errors in these models. Acta Crystallogr. A 47, 110–119.

Kabsch, W., Sander, C., 1983. Dictionary of protein secondary structure: pattern recognition of hydrogen-bonded and geometrical features. Biopolymers 22, 2577–2637.

Kamekura, M., Onishi, H., 1982. Cell-associated cations of the moderate halophile *Micrococcus varians* ssp. *halophilus* grown in media of high concentrations of LiCl, NaCl, KCl, RbCl, or CsCl. Can. J. Microbiol. 28, 155–161.

Kim, F.J., Kim, H.P., Hah, Y.C., Roe, J.H., 1996. Differential expression of superoxide dismutases containing Ni and Fe/Zn in *Streptomyces coelicolor*. Eur. J. Biochem. 241, 178–185.

Kraulis, P.J., 1991. MOLSCRIPT: a program to produce both detailed and schematic plots of protein structures. J. Appl. Crystallogr. 24, 945–949.

Laskowski, R.A., MacArthur, M.W., Moss, D.S., Thornton, J.M., 1993. PROCHECK: a program to check the stereochemical quality of protein structures. J. Appl. Crystallogr. 26, 283–291.

Lee, B., Richard, F.M., 1971. The interpretation of protein structures: estimation of static accessibility. J. Mol. Biol. 55, 379–400.

Le Gall, J., Liu, M.-Y., Payne, W.J., Chang, J., Chang, W.-C., 2000. Post transcriptional expression of superoxide dismutase and nucleoside diphosphate kinase in *Bacillus halodenitrificans*, a nitrite extremophile. Free Radic. Biol. Med. 29 (Supplement 1), S69.

Ludwig, M.L., Metzger, A.L., Pattridge, K.A., Stallings, W.C., 1991. Manganese superoxide dismutase from *Thermus thermophilus*. A structural model refined at 1.8 Å resolution. J. Mol. Biol. 219, 335–358.

Madern, D., Ebel, C., Zaccai, G., 2000. Halophilic adaptation of enzymes. Extremophiles 4, 91–98.

Madern, D., Pfister, C., Zaccai, G., 1995. A single acidic amino acid mutation enhances the halophilic behaviour of malate dehydrogenase from *Haloarcula marismortui*. Eur. J. Biochem. 230, 1088–1095.

Matthews, B.W., 1968. Solvent content of protein crystals. J. Mol. Biol. 33, 491–497.

Merritt, E.A., Murphy, M.E.P., 1994. Raster3D version 2.0: a program for photorealistic molecular graphics. Acta Crystallogr. D 50, 869–873.

Navaza, J., 1994. AMoRe: an automated package for molecular replacement. Acta Crystallogr. A 50, 157–163.

Nicholls, A., Sharp, K.A., Honig, B., 1991. Protein folding and association: insights from the interfacial and thermodynamic properties of hydrocarbons. Proteins: Struct. Funct. Genet. 11, 281–296.

Otwinowski, Z., Minor, W., 1996. Processing of X-ray diffraction data collected in oscillation mode. Methods Enzymol. 276, 307–326.

Parker, M.W., Blake, C.C.F., 1988. Crystal structure of manganese superoxide dismutase from *Bacillus stearothermophilus* at 2.4 Å resolution. J. Mol. Biol. 199, 649–661.

Ramachandran, G.N., Sasisekharan, V., 1968. Conformation of polypeptides and proteins. Adv. Protein Chem. 23, 283–437.

Rice, L.M., Brünger, A.T., 1994. Torsion angle dynamics: reduced variable conformational sampling enhances crystallographic structure refinement. Proteins: Struct. Funct. Genet. 19, 277–290.

Sines, J., Allison, S., Wierzbicki, A., McCammon, J.A., 1990. Brownian dynamics simulation of the superoxide–superoxide dismutase reaction: iron and manganese enzymes. J. Phys. Chem. 94, 959–961.

Stallings, W.C., Pattridge, K.A., Strong, R.K., Ludwig, M.L., 1984. Manganese and iron superoxide dismutases are structural homologs. J. Biol. Chem. 259, 10695–10699.

Stallings, W.C., Pattridge, K.A., Strong, R.K., Ludwig, M.L., 1985. The structure of manganese superoxide dismutase from *Thermus thermophilus* at 2.4 Å resolution. J. Biol. Chem. 260, 16424–16432.

Tainer, J.A., Getzoff, E.D., Beem, K.M., Richardson, J.S., Richardson, D.C., 1982. Determination and analysis of the 2 Å structure of copper, zinc superoxide dismutase. J. Mol. Biol. 160, 181–217.

Ventosa, A., Nieto, J.J., Oren, A., 1998. Biology of moderately halophilic aerobic bacteria. Microbiol. Mol. Biol. Rev. 62, 504–544.

Vriend, G., 1990. WHAT IF: a molecular modeling and drug design program. J. Mol. Graph. 8, 52–56.

Weisser, J., Trüper, H.G., 1985. Osmoregulation in a new haloalkaliphilic *Bacillus* from the Wadi Natrun (Egypt). Syst. Appl. Microbiol. 6, 7–11.

Youn, H.-D., Kim, E.-J., Roe, J.-H., Hah, Y.C., Kang, S.-O., 1996. A novel nickel-containing superoxide dismutase from *Streptomyces* spp. Biochem. J. 318, 889–896.